Vibration and Flutter of Mistuned Bladed-Disk Assemblies

Krishna Rao V. Kaza* and Robert E. Kielb†
NASA Lewis Research Center, Cleveland, Ohio

An analytical model for investigating vibration and flutter of mistuned bladed-disk assemblies is presented. This model accounts for elastic, inertial, and aerodynamic coupling between bending and torsional motions of each individual blade, elastic and inertial couplings between the blades and the disk, and aerodynamic coupling among the blades. The disk is modeled as a circular plate with constant thickness and each blade is represented by a twisted, slender, straight, nonuniform, elastic beam with a symmetric cross section. The elastic, inertia, and tension axes are noncoincident and structural warping of the section is considered explicitly. The blade aerodynamic loading in the subsonic and supersonic flow regimes is obtained from two-dimensional, unsteady cascade theories. All of the possible standing wave modes of the disk and traveling wave modes of the blades are included. The equations of motion are derived by using the energy method in conjunction with the assumed mode shapes for the disk and blades. Continuities of displacement and slope at the blade-disk junction are maintained. The equations are solved to investigate the effects of blade-disk coupling and blade frequency mistuning on vibration and flutter. Results show that the flexibility of practical disks, such as those used for current generation turbofans, does not have a significant influence on either the tuned or mistuned flutter characteristics. However, the disk flexibility may have a strong influence on some of the system frequencies and on forced response.

Nomenclature

A_j = torsional mode shape (j = 1,2,...)
$[A]$ = aerodynamic matrix
a = elastic axis location
a_0 = speed of sound
B_1, B_2 = blade section constants
b, b_R = semichord and reference semichord
C_1, C_2 = warping coefficients
C = blade chord
D = flexural rigidity of the disk
E_d, E_m = Young's modulus of disk and blade materials
$[E], [ED]$ = transformation matrices
e = mass and elastic axis offset
F_1, F_2 = quantities defined in Eq. (13)
f_c = function defined in Eq. (9)
G = shear modulus of elasticity of blade material
$\bar{g}_{arj}, \bar{h}_{arj}$ = complex amplitudes of generalized coordinates out of and in the plane of rotation of the rth interblade phase angle mode
$\bar{g}_{sj}, \bar{h}_{sj}$ = complex amplitudes of generalized coordinates out of and in the plane of rotation of the sth blade
I_{xx}, I_{zz} = blade bending moment of inertia about the centroidal major and minor axes
i = $\sqrt{-1}$
J = torsional constant
k = reduced frequency, $\omega_0 b/V_{\text{eff}} = \omega_0 b/M_{\text{eff}} a_0$
k_1, k_2 = quantities defined in Eq. (13)
k_m = polar mass radius of gyration about elastic axis
k_{m_1}, k_{m_2} = mass radii of gyration about x and z axes
k_A = polar radius of gyration about elastic axis
L = blade length, $= (R_T - R_H)$
L_a = lift per unit blade span
$\ell_{hhr}, \ell_{h\alpha r}$ = lift coefficients due to plunging and pitching motions in rth cascade mode
$\ell_{\alpha hr}, \ell_{\alpha\alpha r}$ = moment coefficients due to plunging and pitching motions in rth cascade mode
$\ell_{hh1n}, \ell_{hh2n}, \ldots$ = coefficients defined in Eq. (17)
M_a = aerodynamic moment per unit blade span
M_r, M_{eff} = relative and effective Mach numbers
M_g, M_h, M_α = number of modes retained in bending motions out of and in the plane of rotation and in torsion
$[M]$ = inertia matrix
m = mass per unit blade length
N, N_D = number of blades in cascade and number of nodal diameters of the disk
n = integer specifying disk nodal diameter, $(= 1,2,\ldots,N_D)$
$[P]$ = stiffness matrix of the system
p_j = quantity defined in Eq. (11)
$[Q]$ = matrix defined in Eq. (29)
$R(\bar{\eta}_d)$ = mode shape function of the disk
R_H, R_T = disk and blade radii
r = radial coordinate and integer specifying cascade mode, $(= 0,1,2,\ldots,N-1)$
s = integer specifying blade, $(= 0,1,2,\ldots,N-1)$
T, T_d, T_t = kinetic energy of blade, disk, and system
t, t_m, t_d = time, thickness of blade, and disk
U, U_d, U_t = strain energy of blade, disk, and system
U_F = blade foreshortening
u, v, w = deformations of elastic axis
$u_d, \bar{u}_d$ = disk deflection, $\bar{u}_d = u_d/R_H$
$\bar{u}_{dacn0}, \bar{u}_{dacN/2}, \bar{u}_{dacn}, \bar{u}_{dasn}$ = amplitude of disk deflection in zero, $N/2$, and nth nodal diameter cosine and sine modes
$u_{dar}, \bar{u}_{dar}$ = amplitude of disk deflection in the rth traveling mode of the disk, $\bar{u}_{dar} = u_{dar}/R_H$
V_a = axial velocity
V_{eff} = effective velocity, $= \sqrt{V_a^2 + \Omega^2 r^2}\cos[90 - \xi - \tan^{-1} V_a/\Omega r]$
W_j = bending mode shape, $j = 1,2,\ldots$
$\{\bar{X}_s\}, \{X\}, \{Y_{ar}\}, \{Y\}$ = column matrices

Presented as Paper 84-0991 at the AIAA/ASME/ASCE/AHS 25th Structures, Structural Dynamics and Materials Conference, Palm Springs, CA, May 14-16, 1984; received July 23, 1984, revision received March 22, 1985. This paper is declared a work of the U.S. Government and therefore is in the public domain.

*Research Scientist, Aeroelasticity Section. Associate Fellow AIAA.
†Research Scientist, System Dynamics Section. Member AIAA.

α = twisting deformation positive about $(-y)$ axis
α_{sj} = complex amplitude of generalized coordinate in torsion of the sth blade ($j=1,2,\ldots$)
α_{arj} = complex amplitude of generalized coordinate in torsion of rth interblade phase angle mode of tuned cascade
β_r = interblade phase angle in rth mode
γ = nondimensional eigenvalue, $=(\omega/\omega_0)^2$
δW = virtual work by aerodynamic loading
$\epsilon_r, \epsilon_\psi$ = strain components, Eq. (20)
$\eta, \eta_d, \bar{\eta}, \bar{\eta}_d$ = blade and disk coordinates; $\eta = r - R_H$, $\eta_d = r$, $\bar{\eta} = \eta/L$, $\bar{\eta}_d = \eta_d/R_H$
λ = warping function
$\bar{\mu}$ = real part of eigenvalue
υ_m, υ_d = Poisson's ratio of blade and disk materials
$\bar{\upsilon}$ = imaginary part of eigenvalue
ξ = pretwist angle
ρ_m, ρ_d, ρ_a = densities of blade and disk materials and air
σ_r, σ_ψ = stress components, Eq. (20)
τ = nondimensional time, $=\omega_0 t$
ψ, ψ_s = angular coordinate of disk and of sth blade
Ω = rotational speed
ω, ω_0 = frequency and reference frequency

Introduction

VIBRATION, aeroelastic stability, and response of bladed-disk assemblies employed in modern aircraft turbofan engines have been among the most difficult analysis problems encountered. The blades are thin and can have a considerable amount of built-in pretwist. As a consequence of pretwist and rotation, the blade natural modes involve coupling between the in-plane (the plane of rotation) and out-of-plane bending and the torsional motions. Another consequence of rotation is that the blades experience steady-state equilibrium loads which in turn require either an explicit or implicit consideration of geometric nonlinear theory of elasticity to adequately model the blade behavior. In addition, the individual blades are structurally coupled through the disk and often through a variety of other connecting parts such as shrouds, dampers, and lacing wires. These problems are further compounded by the presence of small differences between the individual blades, known as structural mistuning.

Unlike the case of a fixed wing, the flow Mach number varies along the blade span and involves unsteady subsonic, transonic, and supersonic flow regimes. The flowfield is three dimensional and also involves aerodynamic interference between adjacent blades within a stage as well as from upstream and downstream stators and rotors.

Because of the complexities mentioned above, the research work in the subject area has been proceeding with simple but progressively refined mathematical models. Vibration of the bladed-disk assemblies with structural coupling has been studied in many publications, for example, Refs. 1-4. Flutter and response using single-degree-of-freedom blade models without structural coupling between blades, including mistuning, are addressed in Refs. 5-7. Structural coupling was considered implicitly in Ref. 8 using twin orthogonal modes. References 9-13 have considered flutter of tuned assemblies with rigid disks. Coupled-disk-shroud flutter was studied in Ref. 14. A finite element formulation was presented in Ref. 15 to study the flutter of bladed-disk systems. References 16 and 17 investigated the effects of mistuning on cascade flutter and response in incompressible, subsonic, and supersonic flow regimes with a rigid disk and a typical section model in which each blade has two degrees of freedom, one bending and one torsion. Effects of blade mistuning on flutter were also investigated in Refs. 18 and 19. Furthermore, the single-degree-of-freedom typical section model used in Ref. 5 was modified in Ref. 20 to include disk flexibility, and a subsonic aerodynamic theory was used to investigate flutter. The two-degree-of-freedom typical section model used in Refs. 16 and 17 was refined in Ref. 21 to include disk flexibility and to study flutter and response.

The typical section model used in Refs. 16, 17, and 21 was found to be adequate to elicit physical understanding of mistuning effects. Parametric studies indicated that structural mistuning has the potential to raise the flutter speed of an advanced turbofan significantly. This potential may be utilized to eliminate the shrouds which adversely affect aerodynamic performance. To obtain more accurate flutter boundaries, including the effects of mistuning, the typical section model was replaced by a beam model with a rigid disk in Ref. 22. The beam model was further extended in Ref. 23 to include blade sweep in order to investigate the possibility of classical flutter in advanced turboprops.

A logical extension to the existing literature is to refine the structural model used in Ref. 22 to include disk flexibility by treating the disk as a circular plate. The purpose of the research in the present paper is to combine such a structural model for the disk with a beam model for each blade in order to study the effects of coupling between disk and blade modes and of blade frequency mistuning on vibration and flutter. The beam model used in Ref. 22 is similar to the one used in Ref. 24, but the effect of warping was considered only partially in an implicit manner. In Ref. 25, the present authors found that the partial inclusion of warping in calculating uncoupled torsional frequencies and mode shapes of twisted rotating turbofan blades is not adequate and, hence, modified the model to include all of the warping effects. This modified beam model will be used herein. The unsteady, two-dimensional, cascade, aerodynamic loads are calculated by Smith's theory[26] in subsonic flow and Adamczyk and Goldstein's theory[27] in supersonic flow with a subsonic leading edge.

The equations of motion are derived by using an energy method in conjunction with assumed mode shapes for the disk and each blade. Continuity of displacements and slopes at the blade-disk junction is maintained. The resulting equations are cast in the form of a standard complex eigenvalue problem from which the vibration and aeroelastic stability characteristics are determined. A computer program is developed to form and solve the complex eigenvalue program. In order to have checks for some special cases at least, the equations and computer program developed in Ref. 22 form special cases of the present ones.

This paper presents an analytical model, the development of the equations of motion and computer program, and some selected results for an advanced fan stage.

Theory

The motion of a bladed-disk assembly with or without mistuning can be expressed in terms of either standing or traveling wave form. Since stability is independent of the wave representation, either representation adequately describes the motion. In most of the published literature[5,16,21,22] on blade flutter of turbomachines, the traveling wave modes are preferred because the unsteady aerodynamic loads are expressed in these modes. This is in contrast to the conventional flutter analysis of airplane wings and vibration of disks in which the standing wave modes are used. However, the present formulation uses both types of modes because the development includes both the blade and the disk flexibility and also is based on the development in Ref. 22. Hence, it will be necessary to understand both the traveling and standing wave mode representations and the relation between them.

To understand the traveling wave modes, consider the vibratory bending motion of each blade of an N-bladed rotor with a rigid disk. For illustration purposes, consider only one bending mode for each blade. Then the cascade has N degrees of freedom. The motion of the system can be expressed in

terms of traveling wave modes each of which is characterized by the phase angle β_r between the adjacent blades. The angle is commonly called the interblade phase angle. The phase angle is restricted to N discrete values, $\beta_r = 2\pi r/N$ where the wave number index $r = 0,1,2,\ldots,(N-1)$. In each of these modes, all blades move with the same amplitude and every adjacent pair moves with the same interblade phase angle.

To understand the standing wave modes and their relation to the traveling wave modes, consider the disk bending deflection perpendicular to the plane of the disk in the traveling wave form as

$$\bar{u}_d = \frac{u_d}{R_H} = \sum_{r=0}^{N-1} R(\bar{\eta}_d)\bar{u}_{dar} e^{i(r\psi + \omega/\omega_0 \tau)} \tag{1}$$

Theoretically, the wave numbers for an elastic disk can have values up to infinity. However, if N blades are attached to the disk and if the number of traveling wave modes is restricted to N, then the wave number index is also limited to $(N-1)$. Thus, the disk with the N attached blades can be characterized by N traveling wave modes. Assuming simple harmonic motion, the real part of Eq. (1) can be rearranged to give the disk deflection in the standing wave form as

$$\bar{u}_d = R(\bar{\eta}_d)\left[\bar{u}_{dac0} + \bar{u}_{dacN/2}\cos\frac{N}{2}\psi + \sum_{n=1}^{N_D}(\bar{u}_{dacn}\cos n\psi + \bar{u}_{dasn}\sin n\psi)\right] e^{i(\omega/\omega_0)\tau} \tag{2}$$

where $N_D = (N-1)/2$ for odd N and $N_D = (N-2)/2$ for even N, and n is the nodal diameter index. Thus, the disk with the N attached blades can be characterized by $0,1,2,\ldots,N_D$ and $N/2$ nodal diameters.

Coordinate Systems

Coordinate systems employed in deriving the equations of motion of the sth blade are shown in Figs. 1 and 2. The axis system X_Ω, Y_Ω, Z_Ω rotates with a constant angular velocity Ω about the X_Ω axis. The Y_Ω axis coincides with the undeformed elastic axis of the blade. The principal axis x of the blade cross section at any point on the elastic axis is inclined to the X_Ω axis by an angle ξ as shown in Fig. 2. The disk elastic deformation u_d, and the blade deformations u, v, w, and α translate and rotate the xyz system to the $x_3y_3z_3$ system.

Motion of a Tuned Bladed-Disk System

Following common practice in the literature, the disk motion is expressed in standing wave modes and the blade motion is expressed, as in Ref. 22, in traveling wave modes. For the disk, using a single quadratic deflection shape along the radius for all of the possible nodal diameter modes, the expression for the motion is given by Eq. (2) with

$$R(\bar{\eta}_d) = \bar{\eta}_d^2 \tag{3}$$

For the blades, assume the number of modes retained in the plane of rotation, in the plane perpendicular to the plane of rotation, and in torsion are M_h, M_g, and M_α, respectively. Then, the motion of the sth blade can be represented as

$$\bar{w} = w/b_R = \sum_{j=1}^{M_h} W_j(\bar{\eta})\bar{h}_{sj}\exp\left[i\left(\frac{\omega}{\omega_0}\right)\tau\right] = \sum_{j=1}^{M_h} W_j(\bar{\eta})\bar{h}_{arj}\exp\left\{i\left[\beta_r s + \left(\frac{\omega}{\omega_0}\right)\tau\right]\right\} \tag{4}$$

$$\bar{u} = u/b_R = \sum_{j=1}^{M_g} W_j(\bar{\eta})\bar{g}_{sj}\exp\left[i\left(\frac{\omega}{\omega_0}\right)\tau\right] + f_c(\bar{\eta})\bar{u}_d\Big|_{\substack{\bar{\eta}_d=1 \\ \psi=\psi_s}} = \sum_{j=1}^{M_g} W_j(\bar{\eta})\bar{g}_{arj}\exp\left\{i\left[\beta_r s + \left(\frac{\omega}{\omega_0}\right)\tau\right]\right\} + f_c(\bar{\eta})\bar{u}_d\Big|_{\substack{\bar{\eta}_d=1 \\ \psi=\psi_s}} \tag{5}$$

$$\alpha = \sum_{j=1}^{M_\alpha} A_j(\bar{\eta})\alpha_{sj}\exp\left[i\left(\frac{\omega}{\omega_0}\right)\tau\right] - \frac{\partial \bar{u}_d}{\partial\psi}\Big|_{\substack{\bar{\eta}_d=1 \\ \psi=\psi_s}} = \sum_{j=1}^{M_\alpha} A_j(\bar{\eta})\alpha_{arj}\exp\left\{i\left[\beta_r s + \left(\frac{\omega}{\omega_0}\right)\tau\right]\right\} - \frac{\partial \bar{u}_d}{\partial\psi}\Big|_{\substack{\bar{\eta}_d=1 \\ \psi=\psi_s}} \tag{6}$$

In Eqs. (4-6), the complex constants $\bar{h}_{sj}$, $\bar{g}_{sj}$, and α_{sj}, which are commonly used in fixed-wing and rotary-wing aeroelasticity, are expressed in terms of the new constants, $\bar{h}_{arj}$, $\bar{g}_{arj}$, and α_{arj} and the interblade phase angle since the aerodynamic loads are expressed in terms of the new constants. The total number of degrees of freedom for the bladed disk system is N times $(1 + M_h + M_g + M_\alpha)$. The function $f_c(\bar{\eta})$ in Eq. (5) is determined by enforcing the continuity of displacement and slope

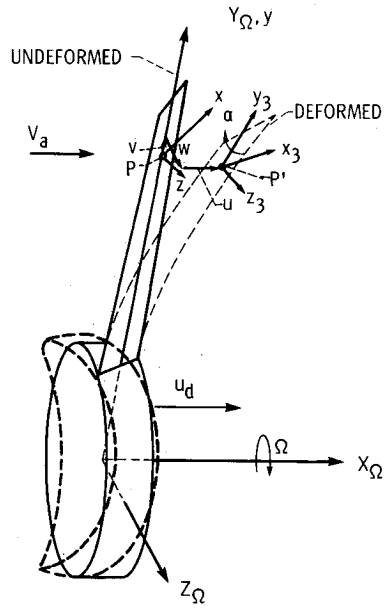

Fig. 1 Blade coordinate systems before and after deformation.

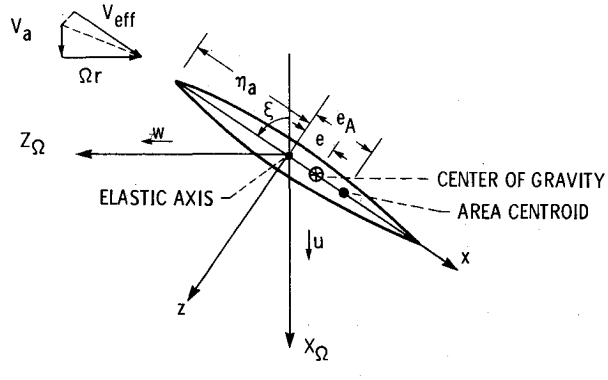

Fig. 2 Coordinate systems of blade cross section.

at the blade-disk junction point

$$\bar{u}\Big|_{\bar{\eta}=0} = \frac{R_H}{b_R}\bar{u}_d\Big|_{\bar{\eta}_d=1} \tag{7}$$

$$\frac{\partial\bar{u}}{\partial\bar{\eta}}\Big|_{\bar{\eta}=0} = \frac{R_H}{b_R}\frac{\partial\bar{u}_d}{\partial\bar{\eta}_d}\Big|_{\bar{\eta}_d=1} \tag{8}$$

These two conditions are satisfied if

$$f_c(\bar{\eta}) = \frac{R_H}{b_R}\left(1+2\bar{\eta}\frac{L}{R_H}\right) \tag{9}$$

In Eqs. (4) and (5), the standard nonrotating orthogonal normal modes in bending for a beam with fixed-free boundary conditions are given by

$$W_j(\bar{\eta}) = \cosh(p_j\bar{\eta}) - \cos(p_j\bar{\eta}) - \frac{(\cos p_j + \cosh p_j)}{(\sin p_j + \sinh p_j)}[\sinh(p_j\bar{\eta}) - \sin(p_j\bar{\eta})] \tag{10}$$

where p_j is calculated from

$$\cos p_j \cosh p_j + 1 = 0 \tag{11}$$

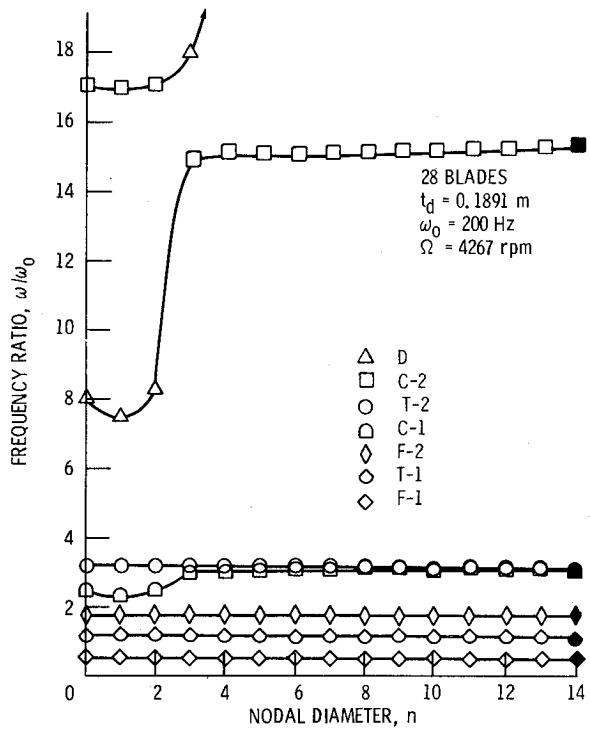

Fig. 3 Frequencies of bladed-disk system, $t_d = 0.1891$ m.

In Eq. (6) the orthogonal nonrotating modes in torsion for a uniform twisted beam with fixed-free boundary conditions are obtained from Ref. 25 and are

$$A_j(\bar{\eta}) = \left[\left(\sinh k_1\bar{\eta} - \frac{k_1}{k_2}\sin k_2\bar{\eta}\right) - \frac{(k_1^2\sinh k_1 + k_1k_2\sin k_2)}{(k_1^2\cosh k_1 + k_2^2\cos k_2)}(\cosh k_1\bar{\eta} - \cos k_2\bar{\eta})\right] \tag{12}$$

where

$$k_1 = \left[\left(\frac{F_1^2}{4}+F_2\right)^{1/2} + \frac{F_1}{2}\right]^{1/2},\quad k_2 = \left[\left(\frac{F_1^2}{4}+F_2\right)^{1/2} - \frac{F_1}{2}\right]^{1/2},\quad F_1 = \frac{24}{1+\nu_m}\left(\frac{L}{c}\right)^2 + \frac{4}{5}\frac{c^2}{t_m^2}\xi'^2,\quad F_2 = 12\frac{\rho_m}{E_m}\frac{L^4}{t_m^2}\omega_{NR}^2 \tag{13}$$

The nonrotating frequency, ω_{NR}, for each mode is obtained from

$$2F_2 + (2F_2 + F_1^2)\cos k_2\cosh k_1 + F_1\sqrt{F_2}\sin k_2\sinh k_1 = 0 \tag{14}$$

In calculating the mode shapes and frequencies, average values of actual blade shape are used for L/c, c/t_m, and ξ' in Eq. (13).

Motion of Mistuned Bladed-Disk System

In the present formulation we consider mistuning only due to nonidentical structural properties of the blades, since the disk thickness is assumed to be uniform. Due to the mistuning there will be coupling between various traveling wave modes or equivalently between the various standing wave modes. However, the general motion of an arbitrarily mistuned system can be expressed as a linear combination of the motions in either traveling or standing wave modes. The disk motion in Eq. (2) is already expressed in terms of the possible nodal diameter modes. The motion of the sth blade is obtained by simply superposing the blade deflections [in Eqs. (4-6)] in the rth traveling mode from $r=0$ to $N-1$.

Aerodynamic Model

For a rigid disk, the motion-dependent aerodynamic lift and moment per unit blade span are expressed in Ref. 22 in terms of four coefficients ℓ_{hhr}, $\ell_{h\alpha r}$, $\ell_{\alpha hr}$, and $\ell_{\alpha\alpha r}$, and blade motions written in a traveling form. These coefficients were calculated by using Smith's theory in subsonic flow and Adamczyk and Goldstein's theory in supersonic flow with a subsonic leading edge. At any radial station, the relative Mach number is a function of in-flow conditions and rotor speed. Most current fan designs have supersonic flow at the blade tip and subsonic flow at the blade root. Consequently, some regions of the blade encounter transonic flow. Since the above theories are not valid in the transonic region, the subsonic theory with $M_{\text{eff}} = 0.9$ for stations in the range $0.9 \le M_{\text{eff}} < 1$ and the supersonic theory with $M_{\text{eff}} = 1.1$ for stations in the range $1.0 \le M_{\text{eff}} \le 1.1$ were used.

For a flexibile disk, the lift and moment expressions can be divided conveniently into two parts: one due to blade motion and the other due to disk motion. The first part flows directly from Ref. 22. The second part can be obtained in two steps. First, express the lift and moment due to disk motion in the traveling wave form represented by Eq. (1) in terms of the four coefficients mentioned earlier. Second, take the real part of the resulting expressions, rearrange the terms, and by assuming simple harmonic motion, derive the expressions for lift and moment per unit span due to disk motion represented by Eqs. (2) and (3) (see also Refs. 13 and 28). Combining these two parts, the lift and moment expressions per unit span of the sth blade can be derived as

$$L_a = -\pi\rho_a b_R^3\omega^2\Bigg\{\sum_{r=0}^{N-1}\left[\ell_{hhr}\left(\frac{b}{b_R}\right)^2\left[\cos\xi\sum_{j=1}^{M_h}W_j(\bar\eta)\bar h_{arj}+\sin\xi\sum_{j=1}^{M_g}W_j(\bar\eta)\bar g_{arj}\right]+\ell_{h\alpha r}\left(\frac{b}{b_R}\right)^3\sum_{j=1}^{M_\alpha}A_j(\bar\eta)\alpha_{arj}\right]\exp\left\{i\left[\left(\frac{\omega}{\omega_0}\right)\tau+\beta_r s\right]\right\}$$
$$+f_c(\bar\eta)\sin\xi\left(\frac{b}{b_R}\right)^2\left[\ell_{hh0}\bar u_{\mathrm{dac}0}+\ell_{hhN/2}\cos\frac{N}{2}\psi_s\bar u_{dacN/2}+\sum_{n=1}^{N_D}\left[(\ell_{hhln}\bar u_{dacn}+\ell_{hh2n}\bar u_{dasn})\cos n\psi_s+(-\ell_{hh2n}\bar u_{dacn}+\ell_{hh1n}\bar u_{dasn})\sin n\psi_s\right]\right]$$
$$\times\exp\left[i\left(\frac{\omega}{\omega_0}\right)\tau\right]+\left(\frac{b}{b_R}\right)^3\sum_{n=1}^{N_D}n[(\ell_{h\alpha 1n}\bar u_{dasn}-\ell_{h\alpha 2n}\bar u_{dacn})\cos n\psi_s-(\ell_{h\alpha 2n}\bar u_{dasn}+\ell_{h\alpha 1n}\bar u_{dacn})\sin n\psi_s]\exp\left[i\left(\frac{\omega}{\omega_0}\right)\tau\right]\Bigg\} \tag{15}$$

$$M_a = -\pi\rho_a b_R^4\omega^2\Bigg\{\sum_{r=0}^{N-1}\left[\ell_{\alpha hr}\left(\frac{b}{b_R}\right)^3\left[\cos\xi\sum_{j=1}^{M_h}W_j(\bar\eta)\bar h_{arj}+\sin\xi\sum_{j=1}^{M_g}W_j(\bar\eta)\bar g_{arj}\right]+\ell_{\alpha\alpha r}\left(\frac{b}{b_R}\right)^4\sum_{j=1}^{M_\alpha}A_j(\bar\eta)\alpha_{arj}\right]\exp\left[i\left(\frac{\omega}{\omega_0}\tau+\beta_r s\right)\right]$$
$$+f_c(\bar\eta)\sin\xi\left(\frac{b}{b_R}\right)^3\left[\ell_{\alpha h0}\bar u_{\mathrm{dac}0}+\ell_{\alpha hN/2}\cos\frac{N}{2}\psi_s\bar u_{dacN/2}+\sum_{n=1}^{N_D}\left[(\ell_{\alpha hln}\bar u_{dacn}+\ell_{\alpha h2n}\bar u_{dasn})\cos n\psi_s+(-\ell_{\alpha h2n}\bar u_{dacn}+\ell_{\alpha h1n}\bar u_{dasn})\sin n\psi_s\right]\right]$$
$$\times\exp\left[i\left(\frac{\omega}{\omega_0}\right)\tau\right]+\left(\frac{b}{b_R}\right)^4\sum_{n=1}^{N_D}n[(\ell_{\alpha\alpha 1n}\bar u_{dasn}-\ell_{\alpha\alpha 2n}\bar u_{dacn})\cos n\psi_s-(\ell_{\alpha\alpha 2n}\bar u_{dasn}+\ell_{\alpha\alpha 1n}\bar u_{dacn})\sin n\psi_s]\exp\left[i\left(\frac{\omega}{\omega_0}\right)\tau\right]\Bigg\} \tag{16}$$

where

$$\ell_{hh1n}=(1/2)[\ell_{hhn}+\ell_{hh(N-n)}]$$
$$\ell_{hh2n}=-(i/2)[\ell_{hhn}+\ell_{hh(N-n)}]$$
$$\vdots$$
$$\ell_{\alpha\alpha 2n}=-(i/2)[\ell_{\alpha\alpha n}+\ell_{\alpha\alpha(N-n)}] \tag{17}$$

The coefficients ℓ_{hhr}, $\ell_{h\alpha r}$, $\ell_{\alpha hr}$, and $\ell_{\alpha\alpha r}$ are calculated for each value of r for specified values of Mach number, reduced frequency, s/c, ξ, and a. Then, the corresponding coefficients ℓ_{hh1n}, ℓ_{hh2n},..., $\ell_{\alpha\alpha 2n}$ for each value of the nodal diameter index n are obtained from Eq. (17). Note that the subscripts r and n represent the interblade phase angle and nodal diameter number, respectively.

Structural Model

The bladed-disk system is idealized as a uniform circular plate with constant thickness to which the blades are rigidly attached. Only the disk out-of-plane bending motion is considered. The blade model is the same as that used in Ref. 22 except that warping of the blade cross sections is explicitly considered. Continuity and slope at the blade-disk junction is enforced as described in the previous section.

Equations of Motion

The strain energy expression for a circular disk[29] is

$$U_d=\int_0^{2\pi}\int_0^{R_H}\Bigg\{\frac{D}{2}\Bigg[\left(\frac{\partial^2 u_d}{\partial r^2}+\frac{1}{r}\frac{\partial u_d}{\partial r}+\frac{1}{r^2}\frac{\partial^2 u_d}{\partial r^2}\right)^2$$
$$-2(1-\nu_d)\frac{\partial^2 u_d}{\partial r^2}\left(\frac{1}{r}\frac{\partial u_d}{\partial r}+\frac{1}{r^2}\frac{\partial^2 u_d}{\partial\psi^2}\right)$$
$$+2(1-\nu_d)\left[\frac{\partial}{\partial r}\left(\frac{1}{r}\frac{\partial u_d}{\partial\psi}\right)\right]^2\Bigg]$$
$$+\frac{1}{2}t_d\left[\sigma_r\left(\frac{\partial u_d}{\partial r}\right)^2+\frac{\sigma_\psi}{r^2}\left(\frac{\partial u_d}{\partial\psi}\right)^2\right]\Bigg\}r\,dr\,d\psi \tag{18}$$

where

$$D=E_d t_d^3/12(1-\nu_d^2) \tag{19}$$

The stress components σ_r and σ_ψ are obtained by solving the following equations:

$$\frac{\partial\sigma_r}{\partial r}+\frac{\sigma_r-\sigma_\psi}{r}+\rho_d\Omega^2 r=0$$
$$\sigma_r=\frac{E_d}{1-\nu_d^2}(\epsilon_r+\upsilon_d\epsilon_\psi),\quad \sigma_\psi=\frac{E_d}{1-\nu_d^2}(\epsilon_\psi+\nu_d\epsilon_r)$$
$$\epsilon_r=\frac{\partial u_d}{\partial r},\quad \epsilon_\psi=\frac{u_d}{r},\quad u_d\Big|_{r=0}=0$$
$$\sigma_r\Big|_{r=R_H}=\frac{N}{2\pi R_H t_d}\int_{R_H}^{R_T}m_b\Omega^2 r\,dr \tag{20}$$

and are

$$\sigma_r=\frac{N}{2\pi R_H t_d}\int_{R_H}^{R_T}m_b\Omega^2 r\,dr+\frac{3+\nu_d}{8}\Omega^2\rho_d(R_H^2-r^2)$$
$$\sigma_\psi=\frac{N}{2\pi R_H t_d}\int_{R_H}^{R_T}m_b\Omega^2 r\,dr+\frac{3+\nu_d}{8}\Omega^2\rho_d R_H^2-\frac{1+3\nu_d}{8}\Omega^2\rho_d r^2 \tag{21}$$

The strain energy of the sth blade follows from Ref. 22 and is

$$U=\frac{1}{2}\int_{R_H}^{R_T}[E_m[C_1\alpha''^2+I_{xx}(u''^2\sin^2\xi+w''^2\cos^2\xi$$
$$+2u''w''\sin\xi\cos\xi)+I_{zz}(u''^2\cos^2\xi+w''^2\sin^2\xi$$
$$-2u''w''\sin\xi\cos\xi)+B_1\alpha'^2\xi'^2-2C_2\alpha''(u''\sin\xi+w''\cos\xi)$$
$$+2B_2(u''\cos u-w''\sin\xi)\alpha'\xi']+GJ\alpha'^2]\,dr \tag{22}$$

The explicit consideration of warping introduces two additional coefficients, C_1 and C_2, and modifies the expression for J:

$$C_1=\iint\lambda^2\,dx\,dz$$
$$C_2=\iint\lambda z\,dx\,dz$$
$$J=\iint\left[\left(z-\frac{\partial\lambda}{\partial x}\right)^2+\left(x+\frac{\partial\lambda}{\partial z}\right)^2\right]dx\,dz \tag{23}$$

The other coefficients in Eq. (22) are defined in Ref. 22.

The kinetic energy of the disk is

$$T_d=\frac{1}{2}\int_0^{2\pi}\int_0^{R_H}\rho_d t_d \dot{u}_d^2 r\,dr\,d\psi \tag{24}$$

The kinetic energy of the sth blade also follows from Ref. 22 and is

$$\begin{aligned}T=\frac{1}{2}\int_{R_H}^{R_T} m\{&(\dot{u}^2+\dot{w}^2+k_m^2\dot{\alpha}^2-2e\dot{u}\dot{\alpha}\sin\xi+2e\dot{w}\dot{\alpha}\cos\xi)\\&+\Omega^2[r^2-2rU_F-2re(u'\cos\xi-w'\sin\xi)\\&-2re\alpha(u'\sin\xi+w'\cos\xi)+w^2+(k_{m_2}^2-k_{m_1}^2)\alpha^2\cos 2\xi\\&-(k_{m_2}^2-k_{m_1}^2)\alpha\sin 2\xi+2e\alpha w\cos\xi-2ew\sin\xi]\}dr\end{aligned} \tag{25}$$

The Coriolis and inertial warping terms are considered to be small and are neglected.

The total strain and kinetic energies of the system are

$$U_t=U_d+\sum_{s=0}^{N-1}U, \qquad T_t=T_d+\sum_{s=0}^{N-1}T \tag{26}$$

The generalized aerodynamic forces are calculated from the following virtual work expression:

$$\delta W=\sum_{s=0}^{N-1}\int_{R_H}^{R_T}(-L_a\sin\xi\delta u-L_a\cos\xi\delta w+M_a\delta\alpha)dr \tag{27}$$

By substituting Eqs. (26) and (27) into Lagrange's equation, the equations of motion of the system are obtained. The final equations are nondimensionalized and cast in a standard eigenvalue form as

$$[P]\{X\}=\gamma[Q]\{X\} \tag{28}$$

where

$$\gamma=\left(\frac{\omega}{\omega_0}\right)^2$$

$$[Q]=[M]+[ED][A][ED]^{-1}$$

$$\{X\}=[ED]\{Y\}$$

$$\{X\}=\begin{Bmatrix}\{\bar{u}_d\}\\\{X_o\}\\\{X_1\}\\\vdots\\\{X_{N-1}\}\end{Bmatrix};\qquad \{Y\}=\begin{Bmatrix}\{\bar{u}_d\}\\\{Y_0\}\\\{Y_1\}\\\vdots\\\{Y_{(N-1)}\}\end{Bmatrix}$$

$$[ED]=\begin{bmatrix}[I] & [0]\\ [0] & [E]\end{bmatrix} \tag{29}$$

Table 1 Disk properties

Radius, R_H, m	0.3876
Thickness, t_d	Varied
Young's modulus, E_d, N/m^2	0.1234
Material density, ρ_d, kg/m^3	4373
Poisson's ratio, ν_d	0.3

$$\{\bar{u}_d\}=\begin{Bmatrix}\bar{u}_{dac0}\\\bar{u}_{dacN/2}\\\bar{u}_{dac1}\\\vdots\\\bar{u}_{dacN_D}\\\bar{u}_{das1}\\\vdots\\\bar{u}_{dasN_D}\end{Bmatrix};\quad \{X_s\}=\begin{Bmatrix}\bar{h}_{s1}\\\bar{h}_{s2}\\\vdots\\\bar{g}_{s1}\\\bar{g}_{s2}\\\vdots\\\alpha_{s1}\\\alpha_{s2}\\\vdots\end{Bmatrix};\quad \{Y_r\}=\begin{Bmatrix}\bar{h}_{ar1}\\\bar{h}_{ar2}\\\vdots\\\bar{g}_{ar1}\\\bar{g}_{ar2}\\\vdots\\\alpha_{ar1}\\\alpha_{ar2}\\\vdots\end{Bmatrix}$$

The matrices $[P]$, $[M]$, and $[A]$ are the stiffness, mass, and aerodynamic matrices of the system. The matrix $[E]$ is defined in Ref. 22.

Results and Discussion

Solution

The flutter boundaries are obtained by solving the standard complex eigenvalue problem, Eq. (28). The relation between the frequency ω and γ is

$$i(\omega/\omega_0)=i\sqrt{\gamma}=\bar{\mu}\pm i\bar{\nu} \tag{30}$$

Flutter occurs when $\bar{\mu}>0$. Vibration characteristics are obtained by setting the aerodynamic matrix $[A]$ to zero.

A computer program was written to assemble and solve the generalized eigenvalue problem. As mentioned previously, the formulation and program have a very wide scope for investigating the effects of disk flexibility and blade frequency mistuning on both vibration and flutter of bladed-disk assemblies. Because of space limitations, only selected results are presented.

Vibration

An advanced unshrouded fan stage (aspect ratio = 3.3) representative of a next-generation fan was chosen for analysis. This fan was analyzed in Ref. 22 by treating the disk as rigid. The disk of this fan consists of a thick hub, a thinner web, and a short thick rim to house the blades. Accordingly, a disk model, consisting of three concentric connected nonuniform annuli would be required for accurate modeling. However, to reduce the complexity of the model, the disk is idealized as a circular plate with uniform thickness. To investigate the effects of disk flexibility on both vibration and flutter, four values are considered for disk thickness. For descriptive purposes, the disk with thicknesses 1.891, 0.1891, 0.0946, and 0.0473 m are designated as very rigid, rigid, flexible, and very flexible disks, respectively. The equivalent thickness for a real practical fan may lie between the values for the rigid and flexible disks. The other properties of the disk are listed in Table 1. The blade properties are the same as those listed in Ref. 22 and, hence, are not repeated here. The design speed of this 28-bladed fan stage is 4267 rpm.

The vibration analyses are performed by using six modes for each of the 28 blades and 28 nodal diameter modes for the disk. The blade modes consists of two modes each in the plane of rotation, in the plane perpendicular to the plane of rotation, and in torsion. The total number of degrees of freedom is $28\times 6+28=196$.

The blade frequencies with disk thickness $t_d=1.891$ m are virtually the same as the blade cantilever frequencies. For this blade, the increase in blade torsional frequency for the first mode due to warping is approximately 3%. This increase is less than that expected from uniform beam results presented in Ref. 22 because of unusual blade taper. However, this mode

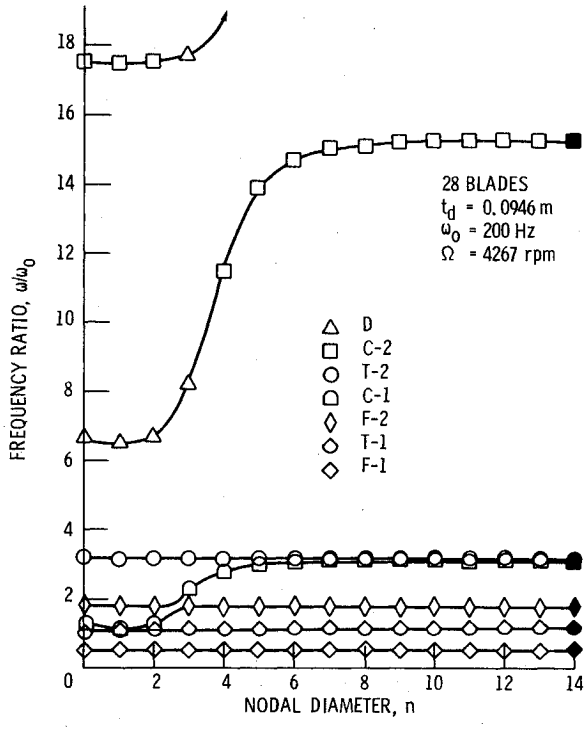

Fig. 4 Frequencies of bladed-disk system, $t_d = 0.0946$ m.

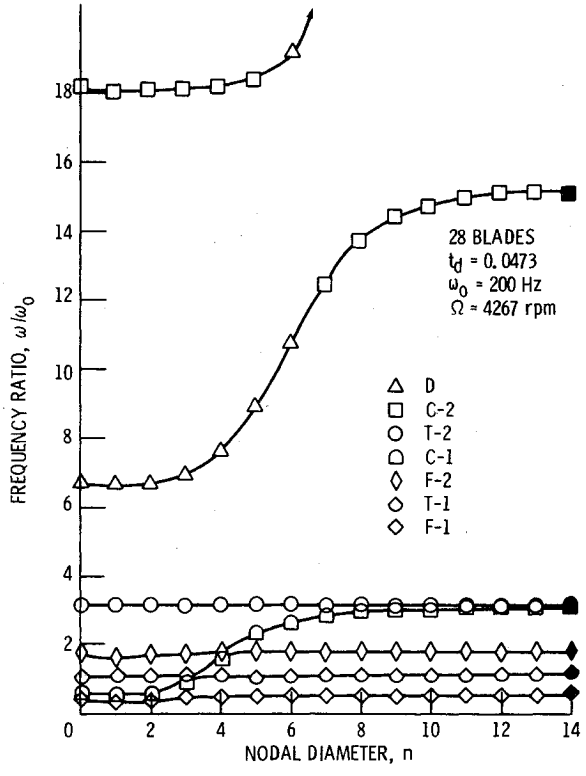

Fig. 5 Frequencies of bladed-disk system, $t_d = 0.0473$ m.

shape with warping is different from that without warping. Thus, the disk with $t_d = 1.891$ m behaves virtually like an infinitely rigid disk. Since the very rigid disk case was analyzed in Ref. 22 for vibration and flutter, the results are not repeated here. The variation of the frequency with nodal diameter index is illustrated in Figs. 3-5 for the other three values of the disk thickness. The frequency ratio is obtained by dividing the frequency by an arbitrarily chosen reference value, $\omega_0 = 200$ Hz. In these figures the frequency ratios are designated as *F, C, T,* and *D* indicating that the blade flatwise, chordwise, torsion, and disk motions, respectively, are predominant in the eigenvectors. The additional numbers 1 and 2 in the designations denote first and second modes. The blade cantilever frequencies are shown by dark symbols. Based on these frequency ratios and the corresponding eigenvectors, which are not shown due to space limitations, several interesting observations are made.

1) For a 28-bladed system, the identification of the predominant motion in the eigenvector was found to be a tedious job. This problem was solved by analyzing a system with 4, 8, 12, and 16 blades since the identification of predominant motion is easier for fewer blades.

2) For each nodal diameter, except for zero and fourteen, each eigenvalue represents a pair of modes and each mode in the pair is a linear combination of $\sin n\psi_s$ and $\cos n\psi_s$. Furthermore, the modes in each pair are orthogonal as expected for a tuned system. The eigenvalues for the zeroth and fourteen nodal diameter represent only one mode. In the zeroth nodal diameter model all of the blades move in phase and in the fourteen nodal diameter mode the phase difference between one blade and its neighbor is 180 deg.

3) Because of the pretwist of the blade, there is a coupling between blade flatwise and chordwise motions and between blade chordwise and disk motions. For the disk with $t_d = 0.1891$ m, it can be seen from Fig. 3 that the coupling between blade chordwise and the disk motions is stronger than that between blade flatwise and disk motions. This is because the disk frequency is in the vicinity of the blade second chordwise frequency. This is contrary to assumptions often made in the published literature dealing with bladed-disk vibrations.

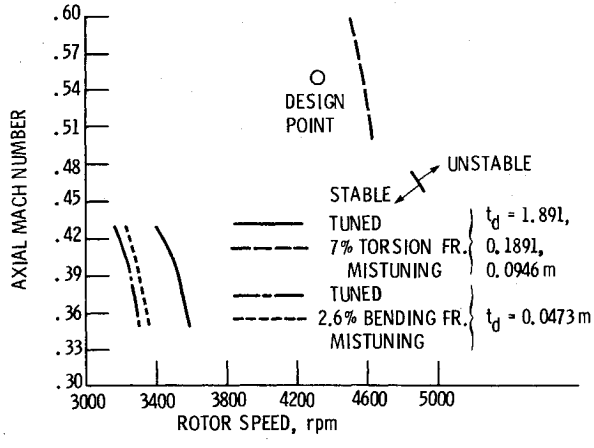

Fig. 6 Effect of disk flexibility on tuned and mistuned bladed-disk system.

4) Comparing the results in Figs. 3-5, the disk frequency decreases with a decrease in disk stiffness, as should be expected. Furthermore, the coupling between the disk and blade motions and blade to blade motions increases as the disk becomes thinner. Alternatively, one could conclude that more of the disk modes couple with the blade modes as the disk flexibility decreases.

5) For the disk with $t_d = 0.1891$ m, it can be seen from Fig. 3 that the coupling between the disk and blades for nodal diameters higher than four is almost negligible.

The effect of alternate mistuning on vibration is investigated. The method used here to vary the frequency from blade to blade is simply to vary either the blade torsional stiffness GJ or the bending stiffness $E_m I_{xx}$. For alternate mistuning the torsional stiffness of the odd numbered blades is increased by 10% and that of even-numbered blades is decreased by 10% from that of a tuned blade system. The result is a frequency variation of approximately 7%. When this mistuning is introduced, the T-1 and T-2 modes in Figs. 3-5 are affected.

The frequency ratios for the T-1 mode alternates between 1.06 and 1.13 and that for the T-2 mode between 2.75 and 2.93. The effect of mistuning is very small in the other frequencies.

A detailed study on vibration of bladed-disk assemblies is presented in Ref. 30. The blade-disk coupling was accomplished by relating the receptances at the junction. The coupling phenomena observed herein is the same as that in Ref. 30.

Flutter of a Tuned Bladed Disk

The advanced fan stage analyzed for vibrations is again considered to investigate flutter behavior including disk flexibility. The solution technique used herein to calculate the flutter boundary is the same as that described in Ref. 22. The correctness of the program was checked by comparing the flutter speed for the case with $t_d = 1.891$ m with that for the rigid disk case in Ref. 22 including all of the warping effects. Next, the effect of disk flexibility on flutter speed is illustrated in Fig. 6. The fan stage is stable if the operating point is to the left of the boundary. For a disk with $t_d = 0.1891$ m the flutter boundary coincides with that for the tuned rigid disk ($t_d = 1.891$ m), indicating that this amount of disk flexibility does not have any influence on flutter. The most unstable interblade phase angle for $t_d = 1891$ m is 64.3 deg, which corresponds to five nodal diameter forward traveling waves. For a disk thickness $t_d = 0.0946$ m, the flutter speed is reduced very slightly. The reduction of flutter speed is more significant when the disk thickness is reduced to 0.0473 m. This degradation in flutter speed is expected because the coupling between disk and blade becomes very strong and reduces blade frequencies (see Fig. 5). In addition, the flutter mode is changed from a predominantly torsional mode for the rigid disk to a predominantly bending mode for a very flexible disk. It should be mentioned that there is no blade bending-torsion coupling inherent in the blades themselves because the center of gravity and elastic axis of any blade are coincident. However, coupling between bending and torsional motions does occur due to the disk flexibility. Furthermore, there is aerodynamic coupling between bending and torsional motions. Thus, flutter involving a predominantly bending mode is not surprising (see also Ref. 16).

Flutter of a Mistuned Bladed Disk

Previous publications[16,17,22] have shown that torsional frequency mistuning could have a significant stabilizing effect on flutter. The effect of mistuning is investigated further herein with the flexible disk model and some selected results are presented in Fig. 6. Alternate blade torsional frequency mistuning of approximately 7% has significantly increased the flutter speed by approximately 30% for the cases with $t_d = 0.1891$ and 0.0946 m. The most predominant unstable interblade phase angle mode for $t_d = 0.1891$ m with mistuning is 90 deg, which corresponds to seven nodal diameter forward traveling waves. The change in the flutter mode interblade phase angle from 64.3 to 90 deg is due to blade frequency mistuning. These findings are in agreement with those in Ref. 22. Again, this amounts to concluding that the disk flexibility does not have much influence on the flutter speed, even in the presence of mistuning. Contrary to these two cases, there is no appreciable improvement in flutter speed due to torsional frequency mistuning for the very flexible disk with $t_d = 0.0473$ m. This might be expected because the predominant motion in the flutter mode is bending rather than torsion. Next, it is natural to ask whether an alternate bending frequency mistuning has any influence on flutter speed. To investigate this, the bending stiffness EI_m of the odd-numbered blades was increased by 10% and that of the even-numbered blades was decreased by 10% from that of a tuned blade. The result is a frequency variation of approximately 2.6%. With this mistuning, the flutter boundaries for the very flexible disk is shown again in Fig. 6. There is a small increase in flutter speed. However, this increase in flutter speed is not as great as that due to alternate torsional mistuning for the rigid disk. It is concluded that mistuning has a modest potential to increase the flutter speed of bending mode even in the presence of mechanical coupling between blades introduced by disk flexibility. It should be emphasized that the flexibility of the disks employed for the current-generation turbofans does not have a significant effect on flutter speed. Still, the flexibility effects should be included in calculating forced response which is sensitive to small changes in system frequencies.

Concluding Remarks

An analytical model and an associated computer program to investigate the effects of disk flexibility on vibration and flutter of tuned and mistuned bladed-disk assemblies are developed. From the parametric studies the following conclusions have been reached.

1) The flexibility of the disks employed for the current-generation turbofans does not have much influence on either tuned or mistuned bladed-disk system flutter. Still, its effect may be significant on forced response which is sensitive to small changes in system frequencies.

2) The flexibility of a very thin disk reduces flutter speed and changes the predominant character of the flutter mode from torsion to bending.

3) Because of the blade pretwist, chordwise motion of the blades is more strongly coupled to the disk motion than the blade flatwise motion. This is contrary to assumptions often made in the published literature on bladed-disk vibrations.

4) A moderate amount of blade frequency mistuning has a significant potential to increase the flutter speed, even in the presence of the mechanical coupling between blades that is introduced by disk flexibility.

References

[1]Wagner, J. T., "Coupling of Turbomachine Blade Vibrations Through the Rotor," *Journal of Engineering for Power,* Vol. 89, Oct. 1967, pp. 502-512.

[2]Dye, R. C. F. and Henry, T. A., "Vibration Amplitudes of Compressor Blades Resulting from Scatter in Blade Natural Frequencies," *Journal of Engineering for Power*, Vol. 91, July 1969, pp. 182-188.

[3]Ewins, D. J., "Bladed Disc Vibration—A Review of Techniques and Characteristics," *Recent Advances in Structural Dynamics,* Univ. of Southampton, U.K., 1980, pp. 187-210.

[4]El-Bayoumy, L. E. and Srinivasan, A. V., "Influences of Mistuning on Rotor-Blade Vibrations," *AIAA Journal,* Vol. 13, April 1975, pp. 460-464.

[5]Whitehead, D. S., "Effect of Mistuning on the Vibration of Turbomachine Blades Induced by Wakes," *Journal of Mechanical Engineering Science,* Vol. 8, March 1966, pp. 15-21.

[6]Whitehead, D. S., "Torsional Flutter of Unstalled Cascade Blades at Zero Deflections," ARC R&M 3429, 1964.

[7]Hanamura, Y. and Tanaka, H., "A Modification of Flutter Characteristics by Changing Elastic Nature of Neighboring Blades in Cascades," Tokyo Joint Gas Turbine Congress, Tokyo, Japan, 1977, pp. 418-427.

[8]Ford, R.A.J. and Foord, C. A., "An Analysis of Aeroengine Fan Flutter Using Twin Orthogonal Vibration Modes," ASME Paper 79-GT-126, March 1979.

[9]Hanamura, Y., "Flutter of Cascading Blade Row," Institute of Space and Aeronautical Science, University of Tokyo, Japan, Vol. 36, Rept. 459, 1971, pp. 1-36.

[10]Shiori, J., "Non-Stall Normal Mode Flutter in Annular Cascades, Part II—Experimental Study," *Transactions of Japan Society of Aeronautical Engineering,* Vol. 1, No. 1, 1958, pp. 26-45.

[11]Rao, B. M. and Kronenbuger, L. Jr., "Aeroelastic Characteristics of a Cascade of Blades," AFOSR-78-1027-TR, Feb. 1978.

[12]Bendiksen, O. and Friedmann, P., "Coupled Bending-Torsion Flutter in Cascades," *AIAA Journal*, Vol. 18, Feb. 1980, pp. 195-201.

[13]Dugundji, J., "Flutter Analysis of a Tuned Rotor with Rigid and Flexible Disks," Massachusetts Institue of Technology, Cambridge, Mass., GT&PDL Rept. 146, July 1979.

[14]Carta, F. O., "Coupled Bladed-Disc-Shroud Flutter Instabilities in Turbo-Jet Engine Rotors," *Journal of Engineering for Power,* Vol. 89, July 1967, pp. 419-426.

[15]Smith, G. C. C. and Elchuri, V., "Aeroelastic and Dynamic Finite Element Analyses of Bladed Shrouded Disk," NASA CR-159728, March 1980.

[16]Kaza, K. R. V. and Kielb, R. E, "Flutter and Response of a Mistuned Cascade in Incompressible Flow," *AIAA Journal,* Vol. 20, Aug. 1982, pp. 1120-1127.

[17]Kielb, R. E. and Kaza, K. R. V., "Aeroelastic Characteristics of a Cascade of Mistuned Blades in Subsonic and Supersonic Flows," *ASME Journal of Vibration, Acoustics, Stress and Reliability of Design,* Vol. 105, Oct. 1983, pp. 425-433.

[18]Srinivasan, A. V. and Fabunmi, J. A., "Cascade Flutter Analysis of Cantilevered Blades," *Journal of Engineering for Gas Turbines and Power,* Vol. 106, No. 1, Jan. 1984, pp. 34-43.

[19]Bendiksen, O. O., "Flutter of Mistuned Turbomachinery Rotors," *Journal of Engineering for Gas Turbines and Power,* Vol. 106, No. 1, Jan. 1984, pp. 25-33.

[20]Srinivasan, A. V., "Influence of Mistuning on Blade Torsional Flutter," NASA CR-165131, Aug. 1980.

[21]Kielb, R. E. and Kaza, K. R. V., "Effects of Structural Coupling on Mistuned Cascade Flutter and Response," *Journal of Engineering for Gas Turbines and Power,* Vol. 106, No. 1, Jan. 1984, pp. 17-24.

[22]Kaza, K. R. V. and Kielb, R. E., "Flutter of Turbofan Rotors with Mistuned Blades," *AIAA Journal,* Vol. 22, Nov. 1984, pp. 1618-1625.

[23]Mehmed, O., Kaza, K. R. V., Lubomski, J. F., and Kielb, R. E., "Bending-Torsion Flutter of a Highly Swept Advanced Turboprop," SAE Paper 82-1361, 1982 Aerospace Congress and Exposition, Anaheim, CA, Oct. 1982.

[24]Houbolt, J. C. and Brooks, G. W., "Differential Equations of Motion for Combined Flapwise Bending, Chordwise Bending, and Torsion of Twisted Nonuniform Rotor Blades," NACA TR 1346, 1958.

[25]Kaza, K.R.V. and Kielb, R. E., "Effects of Warping and Pretwist on Torsional Vibration of Rotating Beams," *Transactions of the ASME Journal of Applied Mechanics,* Vol. 51, No. 4, Dec. 1984, pp. 913-920.

[26]Smith, S. N., "Discrete Frequency Sound Generation in Axial Flow Turbomachines," ARC R&M 3709, 1973.

[27]Adamczyk, J. J. and Goldstein, M. E., "Unsteady Flow in a Supersonic Cascade with Subsonic Leading-Edge Locus," *AIAA Journal,* Vol. 16, Dec. 1978, pp. 1248-1254.

[28]Dugundji, J. and Bundas, D. J., "Flutter and Forced Response of Mistuned Rotors Using Standing Wave Analysis," *AIAA Journal,* Vol. 22, Nov. 1984, pp. 1652-1661.

[29]Timoshenko, S. A., *Theory of Plates and Shells,* McGraw-Hill Book Co., New York, 1940.

[30]Ewins, D. J., "Vibration Characteristics of Bladed Disk Assemblies," *Journal of Mechanical Engineering Science,* Vol. 15, No. 3, 1973, pp. 165-186.